

Unifying the factored and projected gradient descent for quantum state tomography

Yong Wang,¹ Lijun Liu,^{2,*} Shuming Cheng,^{1,3,4,†} Li Li,^{1,3} and Jie Chen^{1,3}

¹*College of Electronic and Information Engineering, Tongji University, Shanghai 201804, China*

²*College of Mathematics and Computer Science, Shanxi Normal University, Linfen 041000, China*

³*Shanghai Research Institute for Intelligent Autonomous Systems, Tongji University, Shanghai 201203, China*

⁴*Institute for Advanced Study, Tongji University, Shanghai, 200092, China*

(Dated: November 6, 2023)

Reconstructing the state of many-body quantum systems is of fundamental importance in quantum information tasks, but extremely challenging due to the curse of dimensionality. In this work, we present an efficient quantum tomography approach that unifies the state factored and projected methods to tackle the rank-deficient issue and incorporates a momentum-accelerated Rprop gradient algorithm to speed up the optimization process. In particular, the techniques of state factorization and P-order absolute map are jointly introduced to ensure both the positivity and rank of state matrices learned in the maximum likelihood function. Further, the proposed state-mapping method can substantially improve the tomography accuracy of other QST algorithms. Finally, numerical experiments demonstrate that the unified strategy is able to tackle the rank-deficient problem and admit a faster convergence and excellent purity robustness. We find that our method can accomplish the task of full tomography of random 11-qubit mixed states within one minute.

I. INTRODUCTION

Quantum state tomography (QST) is a powerful tool to recover full information of the unknown state of many-body quantum systems from measurement statistics, and hence plays an indispensable role in quantum information processing tasks, with wide applications ranging from certifying fundamental principles in quantum theory [1], benchmarking quantum devices [2], to verifying quantum algorithms [3]. However, it is a challenging task due to the curse of dimensionality in the sense that it admits an exponential growth of measurement settings, memory cost, and computing resources as the number of subsystems involved linearly increases [4].

Various approaches have been developed to accomplish the task of QST, and a commonly-used is maximum likelihood estimation (MLE) with no prior knowledge of the state [5]. Since one fundamental physical constraint on the matrices reconstructed from these methods is the positivity, some state mapping techniques are needed. For example, one is to parameterize the state matrix via the Cholesky factorization [6–13] and the other is the state projection which maps negative eigenvalues of the estimated matrix to those of the physical states [14–19]. MLE combining these mapping techniques ensures the positivity, but may results in estimated states biased toward rank-deficient states with at least one or more zero eigenvalues under limited resources [8, 20–22], as does computationally efficient linear regression estimation (LRE) [15, 16, 23]. Subsequently, hedged MLE [20] and Bayesian mean tomography [19, 21] for achieving full-rank estimation, as well as some efficient methods such as compressed sensing [9, 10, 24], permutationally

invariant tomography [25, 26], matrix-product-state tomography [27–29], and neural state tomography [11, 30–32] have also been proposed. However, they either need prior knowledge of the state or are restricted to a special class of states, limiting their application to tomography of unknown states. Thus, a more rank-justified MLE is crucial to estimate the unknown quantum state.

Further, numerous gradient-descent based algorithms for the factored and projected methods have been employed to accelerate the convergence of QST. The well-known examples include the diluted direct gradient [33], conjugate gradient (CG) [34], projected gradient (PG) [17], CG-accelerated PG (CG-APG) [34], momentum-inspired factored gradient [35], stochastic gradient [36], and Riemannian gradient [37]. However, the problematic issues arise that the factored gradient methods have limited convergence speed and reconstruction accuracy, while the projected ones need extra computational resources [34]. Besides, the parameter dependence of some fast gradient algorithms greatly increases the computational burden of state reconstruction.

To address the above issues, here we propose a state-mapping strategy which unifies the technique of factored and projected state mapping and further introduces the momentum-accelerated Rprop (MRprop) gradient descent algorithm to achieve accurate and robust reconstruction. Specifically, noting that replacing the triangular matrix in the factored method by the Hermitian one naturally gives rise to the desired properties of the projected method, we introduce a unified factored and projected method called *P*-order absolute projection. Instead of dropping negative eigenvalues, our method scales by weighting the absolute values of the eigenvalues themselves, such that the devoid of rank-deficient problem and the convergence acceleration of MLE are achieved in the tomography optimization. In contrast, this is also capable to leverage other QST methods, such as the LRE [23] and MLE with CG-APG [34]. To further speed

* lljcelia@126.com

† shuming.cheng@tongji.edu.cn

up the MLE algorithm, the gradient momentum is introduced to accelerate the Rprop gradient descent algorithm with low computational burden. In addition, a product-structured positive operator-valued measure (POVM) is used to measure the quantum system and to reduce storage cost as well as computational resources.

We test our strategy on a large number of random Werner states, ranging from pure states to maximally entangled states. Numerical experiments demonstrate that the unified strategy improves the tomography accuracy and purity robustness, in comparison to either the factored or projected methods. Further, applying the unified method to LRE and MLE with CG-APG achieves similar advantages. Experimental analysis indicates that improvements of the unified strategy stem from the effective mitigation of the rank-deficient issue through the non-loss of state eigenvalue information and proper parameter tuning. Moreover, it is possible to fully tomography random 11-qubit mixed states within one minute, while it takes nearly 15 minutes for superfast MLE with CG-APG tomography of 10-qubit states [34]. The MRprop gradient descent outperforms the iterative MLE (iMLE) [38] and MLE with CG-APG by orders of magnitude in terms of convergence iterations and time, and has a better accuracy than LRE. Finally, our method is robust against the depolarizing noise.

The remainder is organized as follows. Sec. II introduces basic concepts related to QST, including the density matrix, MLE method, state-mapping techniques, and quantum state fidelity. Sec. III details our unified state-mapping strategy, the MRprop gradient algorithm, and the product-structured POVM. Then, the numerical results and analysis are presented in Sec. IV. Finally, the summary and outlook are discussed in Sec. V.

II. QUANTUM STATE TOMOGRAPHY

A. Reconstructing the density matrix

The state of many-body quantum systems is characterized by a density matrix ρ , which is a positive semi-definite (PSD) operator with unit trace, i.e., $\rho \succeq 0$ and $\text{Tr}[\rho] = 1$. Specifically, it can be written as

$$\rho = \sum_i p_i |\psi_i\rangle\langle\psi_i|, \quad (1)$$

where the probability p_i represents the occurrence of pure state $|\psi_i\rangle$, with $\sum_i p_i = 1$ and $p_i \geq 0$. If $\rho = |\psi\rangle\langle\psi|$, then ρ is pure. Otherwise, it is a mixed state. Note that for the N -qubit system, generically, it requires $d^2 - 1$ real parameters to completely determine ρ , where $d = 2^N$ is the dimension of the Hilbert space. It is evident that as the number of qubits N increases, the number of parameters to describe ρ will increase exponentially.

To reconstruct the density matrix ρ in Eq. (1), QST is decomposed of two steps: The first is the measure-

ment procedure which yields the outcome statistics described by probability distributions (PDs) from measuring on identically prepared copies of the unknown quantum state. Each measurement i is modeled as a POVM $\{M_k^i\}$ where the positive operator M_k^i satisfy $\sum_k M_k^i = \mathbb{I}$ for all i , and the probability of each outcome is governed via the Born rule as $P_k^i = \text{Tr}[M_k^i \rho]$. The second is the estimation procedure which estimate a physical $\hat{\rho}$ from those measured PDs. Consequently, it can be formulated as the following optimization problem:

$$\begin{aligned} & \hat{\rho} \\ \text{subject to } & \hat{\rho} \succeq 0 \text{ and } \text{Tr}[\hat{\rho}] = 1, \\ & P_k^i = \text{Tr}[M_k^i \hat{\rho}] = \text{Tr}[M_k^i \rho] \quad \forall M_k^i, \\ & M_k^i \succeq 0 \text{ and } \sum_k M_k^i = \mathbb{I}. \end{aligned} \quad (2)$$

However, it is challenging to directly solve the above problem due to the curse of dimensionality that as the number of qubits linearly increases, it requires an exponential growth of measurement settings to faithfully determine ρ , memory cost to store $\mathbf{P}^i = (P_1^i, \dots, P_n^i)$, and computational resources to process the PDs. In practice, the presence of statistical noise leads us to obtain the frequency $f_k \propto \text{Tr}[M_k \rho]$, instead of the accurate probability of each outcome, which makes the accurate tomography more difficult.

One efficient method to perform state estimation is the MLE [6, 8, 33]. In particular, MLE minimizes the negative log-likelihood function between the observed frequency f_k and the estimated probability $\hat{P}_k = \text{Tr}[M_k \hat{\rho}]$

$$\begin{aligned} & \underset{\hat{\rho}}{\text{minimize}} \quad - \sum_k f_k \ln(\text{Tr}[M_k \hat{\rho}]), \\ \text{subject to } & \hat{\rho} \succeq 0 \text{ and } \text{Tr}[\hat{\rho}] = 1, \\ & M_k \succeq 0 \text{ and } \sum_k M_k = \mathbb{I}, \end{aligned} \quad (3)$$

where $\{M_k\}$ is the POVM, and $\hat{\rho}$ is the estimated physical density matrix. It follows from the convexity of the optimization question that there exists a solution $\hat{\rho}$ to MLE [22, 39]. The MLE method, with no excessive assumptions about the unknown target state and excellent tomography precision, is still the popular tomography method [40], together with experimental verification via the single-ion Zeeman qubit [41] and the polarization states of three photons [42].

B. Mapping techniques to ensure the positivity of estimated states

In the optimization problems (2) and (3), the reconstructed state $\hat{\rho}$ should satisfy the fundamental physical constraint that it is a PSD operator with unit trace, however, this may not be always guaranteed. Thus, to solve this problem, the techniques of state factorization or projection are needed to map the nonphysical states to physical ones.

1. Factorization method

Note that an arbitrary density matrix $\hat{\rho}$ admits the Cholesky factorization,

$$\hat{\rho} = \frac{T_{\hat{\rho}}^{\dagger} T_{\hat{\rho}}}{\text{Tr}[T_{\hat{\rho}}^{\dagger} T_{\hat{\rho}}]}, \quad (4)$$

where the transition matrix $T_{\hat{\rho}}$ is a complex lower triangular matrix and \dagger denotes the complex conjugate operation. Evidently, $\hat{\rho}$ in the form (4) is automatically positive, and hence the QST optimization (3) are reduced to the factored method for searching over $T_{\hat{\rho}}$ without the positivity constraint, instead of $\hat{\rho}$.

It immediately yields that MLE with the state factorization (4) becomes

$$\begin{aligned} & \underset{T_{\hat{\rho}}}{\text{minimize}} \quad - \sum_k f_k \ln \left(\text{Tr} \left[M_k \frac{T_{\hat{\rho}}^{\dagger} T_{\hat{\rho}}}{\text{Tr}[T_{\hat{\rho}}^{\dagger} T_{\hat{\rho}}]} \right] \right), \\ & \text{subject to } M_k \succeq 0 \text{ and } \sum_k M_k = \mathbb{I}, \end{aligned} \quad (5)$$

where $T_{\hat{\rho}}$ could be a nonphysical state. It is remarked that the difficulty in ensuring the positive $\hat{\rho}$ is essentially transferred to optimize the objective function in Eq. (5), and there is evidence to show the improper tomography precision of factored methods [34]. Hence, another technique, called as state projection method, has been proposed to enhance the estimation process [14–19].

2. Projection method

Given a nonpositive Hermitian matrix $\hat{\rho}$ estimated from QST methods, the projection method introduces a map $\mathcal{P}(\cdot)$ which maps its eigenvalues to nonnegative ones with unit sum to produce a physical matrix $\tilde{\rho}$. Indeed, following from the eigenvalue decomposition $\hat{\rho} = Q\Lambda Q^{\dagger}$ where Λ is the diagonal eigenvalue matrix and Q is the corresponding orthogonal matrix, we have

$$\tilde{\rho} = \mathcal{P}(\hat{\rho}) = \mathcal{P}(Q\Lambda Q^{\dagger}) = Q\mathcal{P}(\Lambda)Q^{\dagger} \equiv Q\Sigma Q^{\dagger}, \quad (6)$$

where $\Sigma = \mathcal{P}(\Lambda)$ is a positive diagonal matrix with trace being one, thus satisfying the physical constraints imposed by density matrices. There are many ways to construct the map in Eq. (6), and one possible way is subtracting a coefficient c from all eigenvalues and then zeroing all negative eigenvalues with

$$\Sigma_i = \mathcal{P}(\Lambda_i) = \max(\Lambda_i, 0) \quad (7)$$

for each eigenvalue Λ_i . The well-known examples include the Frobenius norm with alternative projection $\mathcal{F}[\cdot]$ [14] and simplex projection $\mathcal{S}[\cdot]$ [17] to choose a proper coefficient c or the nuclear norm with projection to set c to 0 [19]. For the non-Hermitian matrix $\hat{\rho}$, using $(\hat{\rho} + \hat{\rho}^{\dagger})/2$

naturally gives rise to a Hermitian one which then could be processed in the same procedure.

Then, MLE (3) can be solved with the projection method

$$\begin{aligned} & \underset{\hat{\rho}}{\text{minimize}} \quad - \sum_k f_k \ln(\text{Tr}[M_k \mathcal{P}(\hat{\rho})]), \\ & \text{subject to } M_k \succeq 0 \text{ and } \sum_k M_k = \mathbb{I}, \end{aligned} \quad (8)$$

where $\mathcal{P}(\cdot)$ is any chosen projection method. Essentially, the projection method pulls the estimated matrix $\hat{\rho}$ close to a physical density matrix in the sense of matrix 2-norm [14, 17] and other operator norms [19], to improve the convergence speed and precision. However, dropping some of the negative eigenvalues implies the possibility of loss of state information, making the estimated states biased toward the pure states and thus suffering from the rank-deficient issue.

C. Quantum state fidelity

The estimation performance of QST algorithms can be evaluated via quantum state fidelity which measures the distance between the target and estimated states. Specifically, the quantum fidelity F_q for the estimated state matrix $\hat{\rho}$ and the target ρ is defined as [43]

$$F_q(\hat{\rho}, \rho) = \left(\text{Tr} \left[\sqrt{\sqrt{\hat{\rho}} \rho \sqrt{\hat{\rho}}} \right] \right)^2, \quad (9)$$

the fidelity is symmetric, i.e., $F_q(\hat{\rho}, \rho) = F_q(\rho, \hat{\rho})$. For pure target state, Eq. (9) simplifies to $F_q(\rho = |\psi\rangle\langle\psi|, \hat{\rho}) = \langle\psi|\hat{\rho}|\psi\rangle$. Generally, computing Eq. (9) requires multiple square-root matrix operations, which consumes large computational resources. However, this computing cost can be reduced, if the state information is used.

Noting from the state projection method in Eq. (6) that $\tilde{\rho} = \mathcal{P}(\hat{\rho}) = Q\Sigma Q^{\dagger}$, we have

$$\begin{aligned} F_q(\tilde{\rho}, \rho) &= \left(\text{Tr} \left[\sqrt{Q\sqrt{\Sigma}Q^{\dagger}\rho Q\sqrt{\Sigma}Q^{\dagger}} \right] \right)^2 \\ &= \left(\text{Tr} \left[\sqrt{Q'\Sigma'Q'^{\dagger}} \right] \right)^2 \\ &= \left(\text{Tr} \left[Q'\sqrt{\Sigma'}Q'^{\dagger} \right] \right)^2 = \left(\sum_i \sqrt{\Sigma'_i} \right)^2. \end{aligned} \quad (10)$$

The second equality follows from the eigenvalue decomposition $Q\sqrt{\Sigma}Q^{\dagger}\rho Q\sqrt{\Sigma}Q^{\dagger} = Q'\Sigma'Q'^{\dagger}$ with the orthogonal matrix Q' and nonnegative diagonal matrix Σ' . Obviously, the fidelity (10) needs one single matrix-decomposition operation, thus reducing much computational complexity.

III. UNIFIED FACTORED AND PROJECTED GRADIENT ALGORITHM

As mentioned above, it becomes limited performance for the traditional QST approaches with the factored and/or projected gradient algorithm to tomography multi-qubit system with a large number of qubits. In this section, we present an MLE scheme which employs the unified factored and projected gradient descent (UGD) algorithm to achieve fast accurate state reconstruction. Surprisingly, it is found that it can achieve the full tomography of random 11-qubit mixed states within one minute, while it takes nearly 15 minutes for superfast MLE with CG-APG tomography of 10-qubit states [34].

In our scheme, the state mapping technique is constructed as a unification of the factored and projected methods that weighting of the absolute values of the eigenvalues is parametrically adjusted to mitigate the rank-deficient issue. Then, we design the MRprop algorithm to perform tomography optimization, which has the advantage of fast convergence and time saving. Additionally, the product-structured POVM is employed to measure the quantum system and yield estimated probabilistic data, which reduces storage cost and computational complexity. The estimated state matrix is benchmarked via quantum state fidelity (9). The details are described below.

A. Unified state-mapping strategy

We present a simple and efficient method which combines the state factorization with state projection to map the output matrix $T_{\hat{\rho}}$ to a physical state $\hat{\rho}$.

Note first that if the matrix $T_{\hat{\rho}}$ is Hermitian, the factored method has

$$\begin{aligned}\hat{\rho} &= \frac{T_{\hat{\rho}}^{\dagger} T_{\hat{\rho}}}{\text{Tr}[T_{\hat{\rho}}^{\dagger} T_{\hat{\rho}}]} = \frac{Q\Lambda Q^{\dagger} Q\Lambda Q^{\dagger}}{\text{Tr}[Q\Lambda Q^{\dagger} Q\Lambda Q^{\dagger}]} \\ &= \frac{Q\Lambda^2 Q^{\dagger}}{\text{Tr}[\Lambda^2]} = Q\Sigma Q^{\dagger},\end{aligned}\quad (11)$$

where $T_{\hat{\rho}}$ admits the eigenvalue decomposition $Q\Lambda Q^{\dagger}$, and $\Sigma = \Lambda^2/\text{Tr}[\Lambda^2]$ is automatically a nonnegative diagonal matrix with unit trace. This can be regarded as a unified strategy which first uses a simple projection method to process the transition matrix $T_{\hat{\rho}}$ and simultaneously use the state factorization method to output a physical matrix $\hat{\rho}$ from the processed $T_{\hat{\rho}}$.

Following then from the state projection (6), we are able to easily generalize the above result to

$$\hat{\rho} = \frac{\mathcal{P}(T_{\hat{\rho}}^{\dagger})\mathcal{P}(T_{\hat{\rho}})}{\text{Tr}[\mathcal{P}(T_{\hat{\rho}}^{\dagger})\mathcal{P}(T_{\hat{\rho}})]} = \frac{Q\mathcal{P}(\Lambda)^2 Q^{\dagger}}{\text{Tr}[\mathcal{P}(\Lambda)^2]}.\quad (12)$$

Here we introduce a new class of map methods: P -order

absolute map defined as

$$\mathcal{A}(T_{\hat{\rho}})_P = Q|\Lambda|^{P/2}Q^{\dagger},\quad (13)$$

where the tunable parameter P can be used to adjust the weighting of different eigenvalues of Λ , and it immediately gives rise to P -order absolute projection

$$\hat{\rho} = \mathcal{A}[\cdot]_P = \frac{Q|\Lambda|^P Q^{\dagger}}{\text{Tr}[|\Lambda|^P]}.\quad (14)$$

It is easy to find Eq. (11) is a special case of $\mathcal{A}[\cdot]_P$ with $P = 2$. The parameter P controls the tendency of the estimated state; a small P reduces the variance between eigenvalues and tends to full-rank estimation, and conversely tends to rank-deficient estimation, thus the availability of a suitable P makes the estimated state possess a more reasonable rank. Since more parameter degrees of freedom is assigned to the unified state-mapping method (14), it is suitable for handle different scenarios to meet different tomography needs, such as specific full-rank estimation or rank-deficient estimation.

In this way, the protocol not only joints the factored and projected mapping methods, but more importantly, it utilizes the weighting of the absolute values of the eigenvalues themselves to retain the full eigenvalue information, and effectively handles negative eigenvalues instead of setting them to zero, which effectively mitigates the rank-deficient issue through proper parameter tuning. It is interesting to note that this state-mapping technique can also be applied to known QST algorithms, such as LRE and MLE with CG-APG, to allow for a significant improvement in the tomography precision, supported by the experiments in Sec. IV B.

Finally, it is remarked that there exists an alternate way to combine these two methods in which the factored method is used in the early stage to achieve a fast convergence and then the projected method is employed in the latter stage to improve the tomography precision [34]. However, our numerical results in Secs. IV C and IV D display that it becomes inefficient to tomography the large-qubit states due to the use of CG optimization that requires linear search, and the issues about the switching conditions between these two methods and the computational cost remain to be examined carefully. Besides, the approach is not optimized for eigenvalues and is still limited by the rank-deficient issue of the factored and projected methods.

B. Momentum-accelerated Rprop gradient algorithm

Then, the MRprop gradient algorithm is employed to accelerate the state estimation of the MLE method with the unified state-mapping strategy. The Rprop gradient descent algorithm updates the model parameters based only on the sign of the gradient, the update of the step size depends on two consecutive changes in the gradient; a consistent direction enlarges the step size and vice

Algorithm 1: MRprop gradient algorithm with P -order absolute projection

Input: $f_k, M_k, \theta_0 \in \mathbb{R}^{d^2}$, $lr=1e-3$, $\eta_+=1.14$, $\eta_-=0.66$,
 $\tau_{\max}=50$, $\tau_{\min}=1e-6$, $\mu=1e-4$

Output: $\hat{\rho}(\theta_t)$

```

1 Initialize  $\theta_0$  randomly,  $\eta_0 = lr$ ;
2 for  $t \leftarrow 1, \dots$ , do
3    $\hat{\rho}_t(\theta_{t-1}) \leftarrow \mathcal{A}[T_{\hat{\rho}}(\theta_{t-1})]_P$ ;
4    $f_t(\theta_{t-1}) \leftarrow -\sum_k f_k \ln(\text{Tr}[M_k \hat{\rho}_t(\theta_{t-1})])$ ;
5    $g_t \leftarrow \nabla_{\theta} f_t(\theta_{t-1})$ ;
6   for  $i \leftarrow 0$  to  $d^2 - 1$  do
7     if  $g_{t-1}^i g_t^i > 0$  then
8        $\eta_t^i \leftarrow \min\{\eta_{t-1}^i \eta_+, \tau_{\max}\}$ ;
9     else
10      if  $g_{t-1}^i g_t^i < 0$  then
11         $\eta_t^i \leftarrow \max\{\eta_{t-1}^i \eta_-, \tau_{\min}\}$ ;
12        if  $f_t > f_{t-1}$  then
13           $g_t^i \leftarrow -g_t^i$ 
14        else
15           $g_t^i \leftarrow 0$ ;
16        end
17      else
18         $\eta_t^i \leftarrow \eta_{t-1}^i$ ;
19      end
20    end
21  end
22  if  $\mu > 0$  then
23     $m_t \leftarrow m_{t-1} \mu + \eta_t \text{sign}(g_t)$ ;
24     $\theta_t \leftarrow \theta_{t-1} - m_t$ ;
25  else
26     $\theta_t \leftarrow \theta_{t-1} - \eta_t \text{sign}(g_t)$ ;
27  end
28   $g_{t-1} \leftarrow g_t$ ;
29 end

```

versa decreases it [44]. The Rprop algorithm has the advantages of computational simplicity and fast convergence. We introduce the gradient momentum here to ensure stable and faster convergence, and the procedure of the MRprop gradient algorithm with P -order absolute projection is shown in Algorithm 1.

In addition to the gradient momentum, we also add the judgment on the change of the objective function. If the gradient change is opposite and the function value is greater than the last one, then the gradient is inverted, which further speeds up the convergence of the algorithm. The comparison of our developed method with other QST algorithms is showcased in Secs. IV C, IV D, and IV E.

C. POVM with product-structure

Suppose a POVM $\{M_k\}_{k=1}^K$ is performed on each qubit. Then, the product structure of single-qubit POVM is used to form a general general POVM $\{M_{\mathbf{k}}\}$ for the N -qubit state where $\mathbf{k} = (k_1, \dots, k_N)$ with $k_i \in \{1, \dots, K\}$ and $M_{\mathbf{k}} = M_{k_1} \otimes \dots \otimes M_{k_N}$. The number

of measurement elements $\{M_{\mathbf{k}}\}$ is K^N , thus yielding a K^N -dimensional PD.

For any N -qubit POVM in the above product structure, the tensor product and trace operations for obtaining $P_{\mathbf{k}} = \text{Tr}[M_{\mathbf{k}} \rho]$ can be converted into the product of matrices. We take the 2-qubit state as an example. Given matrices $M_i = \begin{bmatrix} a_i & b_i \\ c_i & d_i \end{bmatrix}$ and $\rho = \begin{bmatrix} A & B \\ C & D \end{bmatrix}$, where A, B, C, D are block matrix elements, there is

$$\begin{aligned}
P_{(i,j)} &= \text{Tr}[(M_i \otimes M_j) \rho] \\
&= \text{Tr} \left[(M_i \otimes M_j) \left(\begin{bmatrix} 1 & 0 \\ 0 & 0 \end{bmatrix} \otimes A + \begin{bmatrix} 0 & 1 \\ 0 & 0 \end{bmatrix} \otimes B + \dots \right) \right] \\
&= a_i \text{Tr}[M_j A] + b_i \text{Tr}[M_j B] + c_i \text{Tr}[M_j C] + d_i \text{Tr}[M_j D] \\
&= \mathcal{V}_{M_i}^T [\mathcal{V}_A \quad \mathcal{V}_B \quad \mathcal{V}_C \quad \mathcal{V}_D]^T \mathcal{V}_{M_j}. \tag{15}
\end{aligned}$$

where \mathcal{V}_X is the column vectorization of matrix X , such as $\mathcal{V}_{M_i}^T = [a \ b \ c \ d]$.

This form can greatly reduce the computational and storage costs, which has been verified in [34], the cost of computing the probabilities is reduced from $O(K^N 4^N)$ to $O(K^{N+1})$. Therefore, we utilize the product-structured POVM in all tested QST algorithms.

IV. NUMERICAL EXPERIMENTS AND RESULTS

We examine our MLE method with the UGD algorithm on a large number of multi-qubit states with a wide range of purity. Specifically, the target states are chosen as

- the N -qubit states

$$\rho = p|\psi\rangle\langle\psi| + \frac{1-p}{d}\mathbb{I} \tag{16}$$

with $0 \leq p \leq 1$ and $d = 2^N$. And the pure state $|\psi\rangle$ belongs to the random state set $\{|\Psi\rangle\}$ where

$$|\Psi\rangle = \sum_{k=0}^{d-1} \Psi_k |k\rangle \tag{17}$$

with the coefficients Ψ_k being sampled from $\{0, 1, i\}$. It is obvious that the set $\{|\Psi\rangle\}$ contains product states, GHZ, and W states.

- the N -qubit pure state $|\psi\rangle$ passing through depolarizing channel

$$\rho = (1-\lambda)|\psi\rangle\langle\psi| + \frac{\lambda}{d}\mathbb{I}, \tag{18}$$

where the noise strength $0 \leq \lambda \leq 1$, and the pure state $|\psi\rangle$ from the above state set $\{|\Psi\rangle\}$ (17). Note that though this class is equivalent to Eq. (16), the target states used to benchmark the QST algorithms are distinct in the sense that the former are pure states while the latter chooses states after depolarizing channel.

Numerical experiments are then performed to study the following problems:

- P1. How does the technique of state factorization and/or projection affect the performance of MLE with MRprop and even other QST algorithms?
- P2. What is the essential reason for the improvements of the unified mapping strategy?
- P3. Is MLE with UGD capable of reconstructing a large number of multi-qubit states, ranging from pure states sampled from the state set $\{|\Psi\rangle\}$ to more general mixed states?
- P4. Are there advantages over previous QST methods with various optimization algorithms, in terms of the tomography precision, time, and iteration, when MLE with UGD is used?
- P5. Is MLE with UGD robust towards noise, such as depolarizing noise?

A. Experimental setups

The single-qubit POVM in this paper is chosen as $\{M_a = 1/4 (\mathbb{I} + \mathbf{s}_a \cdot \boldsymbol{\sigma})\}_{a \in \{0,1,2,3\}}$ with

$$\begin{aligned} \mathbf{s}_0 &= \left(\frac{1}{\sqrt{3}}, \frac{1}{\sqrt{3}}, \frac{1}{\sqrt{3}} \right), \quad \mathbf{s}_1 = \left(-\frac{1}{\sqrt{3}}, -\frac{1}{\sqrt{3}}, \frac{1}{\sqrt{3}} \right), \\ \mathbf{s}_2 &= \left(-\frac{1}{\sqrt{3}}, \frac{1}{\sqrt{3}}, -\frac{1}{\sqrt{3}} \right), \quad \mathbf{s}_3 = \left(\frac{1}{\sqrt{3}}, -\frac{1}{\sqrt{3}}, -\frac{1}{\sqrt{3}} \right), \end{aligned} \quad (19)$$

where $\boldsymbol{\sigma} = (\sigma_1, \sigma_2, \sigma_3)$ are the Pauli operator vector. Note that our method can be easily applied to the case involving multiple POVMs on each qubit and adaptive local measurements. Here, in order to save computational cost and to easily compare with other QST algorithms, we are restricted to the above fixed tetrahedral POVM.

The initial density matrices of all tested QST algorithms are randomly initialized, and the numerical experiments are tested on the computer with single Intel(R) Core(TM) i7-12700KF CPU @ 3.60GHz with 64GB RAM, and single NVIDIA GeForce RTX 3090 Ti GPU with 24GB RAM. All QST algorithms are based on the PyTorch 2.01 and CUDA 11.8, and utilize the GPU as well as the product structure of POVM to speed up operations. The codes are available at [github:QST-UGD](https://github.com/QST-UGD) [45].

We further employ the convergence time [10, 23, 34] and number of iterations [11, 46] to evaluate the learning performance of QST algorithms, together with quantum fidelity for their tomography precision. Specifically, the convergence time is defined as the minimum time accumulated by the algorithm to obtain the learned density matrix during each iteration, while the iteration is one

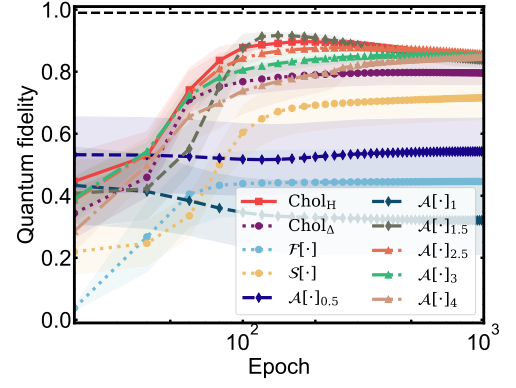


FIG. 1. The tomography convergence of our MLE with MProp based on ten state-mapping methods, with the 10^9 measurement samples. Each experiment is implemented by reconstructing 30 9-qubit Werner states (16) with random pure states and uniformly distributed p . The solid curve denotes the mean fidelity and the shaded area is the half standard deviation around the mean.

density matrix reconstruction, excluding the fidelity calculation. Note that the actual algorithm runtime is inevitably affected by the computing device, but the number of iterations is not. The maximum number of iterations is defaulted as 1000, and the algorithm stops when the state fidelity achieves at 0.99.

B. The better performance of the unified state-mapping strategy

We first show the improvements of the unified strategy by comparing its tomography convergence and precision, as well as purity robustness, to other factored or projected methods acting on our MLE with MProp, LRE [23], and MLE with CG-APG [34] algorithms, and then analyze the reasons for performance improvements in terms of the matching of state eigenvalues.

A total of ten state-mapping techniques are considered:

- the factorization method with the complex lower triangular matrix Chol_Δ (4),
- the $\mathcal{F}[\cdot]$ and $\mathcal{S}[\cdot]$ projection methods (7),
- the simple unified method Chol_H (11),
- the unified method based on P -order absolute projection $\mathcal{A}[\cdot]_P$ (14), with $P = 0.5, 1, 1.5, 2.5, 3$, and 4. Here, $\mathcal{A}[\cdot]_2$ is equivalent to Chol_H .

1. Tomography convergence improvement

We test various mapping methods on our MLE with MProp, by reconstructing the randomly generated 9-qubit Werner states (16) with the 10^9 measurement samples.

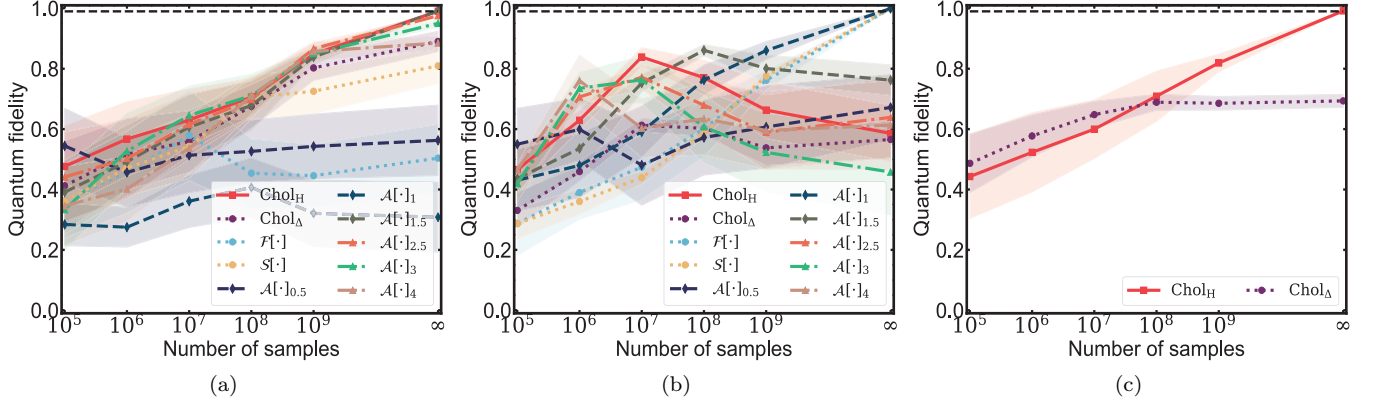


FIG. 2. The tomography precision of our MLE with MProp (a), LRE (b), and MLE with CG-APG (c) based on different state-mapping methods, with the varying sample size. All three QST algorithms do the tomography of 9-qubit random Werner states. Given the sample size of 10^5 , 10^6 , 10^7 , 10^8 , 10^9 , and infinite, each experiment is implemented by reconstructing 30 Werner states (16) with random pure states and uniformly distributed p . The solid curve denotes the mean fidelity and the shaded area is the half standard deviation around the mean.

The results in Fig. 1 demonstrate that P -order absolute projection $\mathcal{A}[\cdot]_P$ with $P > 1$ holds better convergence and final tomography precision, with the best performance when the P is taken to be 2. The factored method Chol_Δ converges fast in the early stage but loses precision, while the projected methods $\mathcal{F}[\cdot]$ and $\mathcal{S}[\cdot]$ do not provide the advantage of convergence speed and tomography precision in our experiments.

2. Tomography precision improvement

We then extend the mapping experiments to three QST algorithms, with the sample size of 10^5 , 10^6 , 10^7 , 10^8 , 10^9 , and infinite case where the measurement statistics is $f_k = \text{Tr}[M_k \rho]$ without noise. The numerical experiments indicate that the unified state-mapping method is powerful to improve the tomography precision of our MLE with MProp, as well as other QST algorithms, such as LRE and MLE with CG-APG.

In particular, it is shown in Fig. 2(a) that unified $\mathcal{A}[\cdot]_P$ with $P > 1$ for our MLE with MProp outperforms other mapping techniques, including Chol_Δ , $\mathcal{F}[\cdot]$, and $\mathcal{S}[\cdot]$, in the sense that a much higher fidelity is achieved with $\mathcal{A}[\cdot]_P$. In terms of tomography fidelity and computational efficiency, the near-optimal parameter P for MLE with MProp is 2, which is equivalently replaced with Chol_H .

Moreover, the unified mapping techniques are also useful to improve the tomography precision of LRE and MLE with CG-APG, supported with the numerical evidence displayed in Fig. 2(b) and (c). It is interesting to note that the near-optimal P is 1 for LRE, other parameters can over-scaling the eigenvalues leading to poor results, and $\mathcal{F}[\cdot]$ and $\mathcal{S}[\cdot]$ rounding off negative eigenvalues leads to loss of state information. For MLE with CG-APG, we are oriented only to the factored method, where

Chol_Δ and Chol_H are used. The results in Fig. 2(c) show that the matrix construction of the factored method is crucial for the tomography precision, and that the form of Hermitian used in this paper utilizes projection features to accelerate convergence. It is conjectured that any generalized symmetric matrices possess similar performance, awaiting more research in the future.

3. Purity robustness improvement

We continue to study how these mapping methods are affected by the state structure, which is measured by the purity defined as $\text{Tr}[\rho^2] \in [0, 1]$. Similar to the experiment setting in Sec. IV B 2, we test MLE with MProp, LRE, and MLE with CG-APG based on ten mapping methods by reconstructing the random Werner states with a wide range of purity. Here, the state purity is fully determined by the uniformly distributed parameter p , ranging from 0 to 1.

In Fig. 3(a), we find that unified $\mathcal{A}[\cdot]_P$ for our MLE with MProp, the growth of P causes the purity of states with high precision to move from low to purity-independent (Chol_H and $\mathcal{A}[\cdot]_{1.5}$) and then to high, i.e., from biased full-rank estimation, to rank-justified, and finally to rank-deficient estimation. In contrast, existing methods of factored and projected tend towards rank-deficient estimation. Moreover, it is found in Fig. 3(b) that for LRE algorithm, $\mathcal{A}[\cdot]_1$ has an equally great robustness as $\mathcal{F}[\cdot]$ and $\mathcal{S}[\cdot]$. For MLE with CG-APG algorithm displayed in Fig. 3(c), the factored method using Hermitian matrices exhibits excellent robustness with respect to the lower triangular form.

The purity reflects the eigenvalue distribution of the density matrix, and the excellent purity robustness of the unified strategy implies its great eigenvalue matching, which is the source of its superior performance against

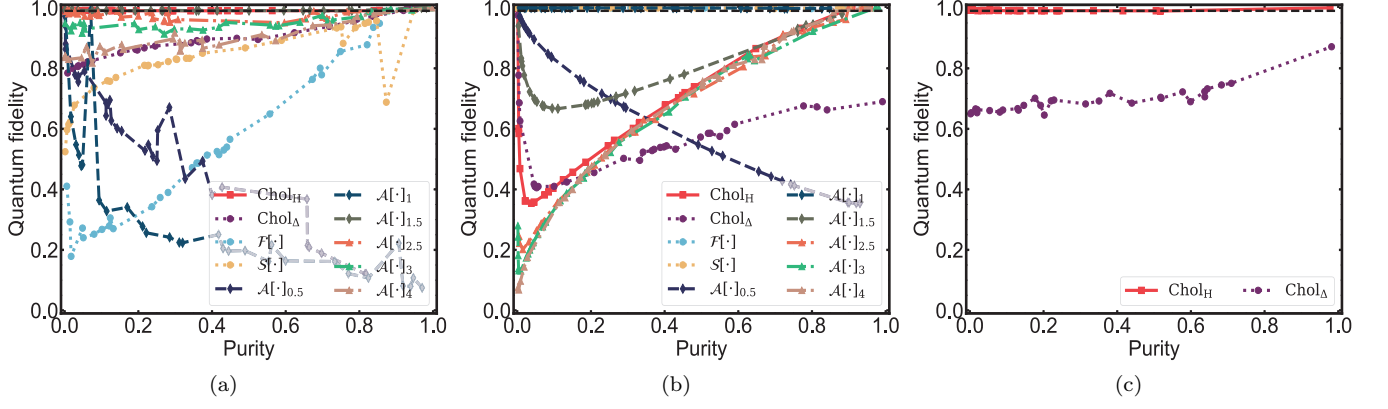


FIG. 3. The purity robustness of our MLE with MProp (a), LRE (b), and MLE with CG-APG (c) algorithms based on the ten mapping methods without sample noise. Again, three QST algorithms are tested on 9-qubit Werner states. Each experiment is implemented by reconstructing 30 Werner states (16) with random pure states and uniformly distributed p . And the state purity $\text{Tr}[\rho^2]$ is fully determined by the parameter p , ranging from 0 to 1.

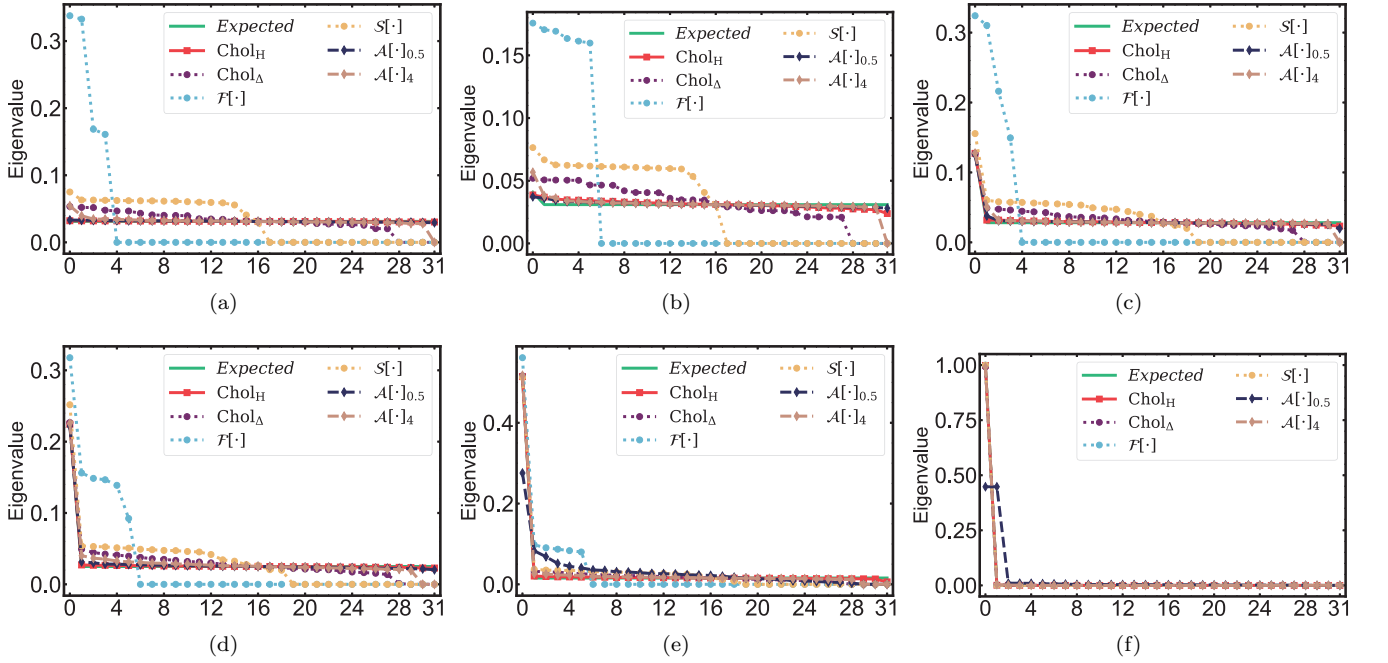


FIG. 4. The eigenvalue matching of our MLE with MProp to 5-qubit Werner states with W state and p of 0 (a), 0.01 (b), 0.1 (c), 0.2 (d), 0.5 (e), and 1 (f). Here, considering the finite iteration and noiseless case, the mapping method is reduced to Chol_H , Chol_Δ , $\mathcal{F}[\cdot]$, $\mathcal{S}[\cdot]$, $\mathcal{A}[\cdot]_{0.5}$, and $\mathcal{A}[\cdot]_4$.

other mapping methods, as illustrated below.

4. Performance improvement analysis

We next analyze the reasons for improvements of the unified strategy in terms of the effect of matching the eigenvalues of the density matrix. The target states are 5-qubit Werner states with W state and p of 0, 0.01, 0.1,

0.2, 0.5, and 1. The W state is included in (17) as

$$|W\rangle = \frac{1}{\sqrt{N}}(|100\dots\rangle + |010\dots\rangle + \dots + |\dots 001\rangle), \quad (20)$$

here, for simplicity, we only analyze the eigenvalue matching of our MLE with MProp algorithm for the six mapping methods Chol_H , Chol_Δ , $\mathcal{F}[\cdot]$, $\mathcal{S}[\cdot]$, $\mathcal{A}[\cdot]_{0.5}$, and $\mathcal{A}[\cdot]_4$ and under no noise.

As shown in Fig. 4, by arranging all the expected and estimated eigenvalues in descending order, we can clearly

observe that the unified Chol_H fits the expected eigenvalues almost perfectly under all tested purities, demonstrating its strong ability against the rank-deficient issue, and the unified strategy under 0.5 and 4 is slightly defective. It is worth noting that, as expected, the factored method Chol_Δ , and the projected methods $\mathcal{F}[\cdot]$ and $\mathcal{S}[\cdot]$, inevitably exist zero eigenvalues (the rank-deficient issue) even though there are no zeros in the expected eigenvalues. This rank-deficient issue occurs most severely with $\mathcal{F}[\cdot]$ and $\mathcal{J}[\cdot]$, and with relatively little impact on Chol_Δ .

From the above analysis, our unified strategy effectively mitigates the rank-deficient issue by matching almost all eigenvalues excellently under suitable parameters, which gives rise to the enhanced tomography precision and purity robustness in Sec. IV B 2 and IV B 3 above. The existing mapping methods, on the other hand, inevitably yield zero eigenvalues and missing partial state information unless pure states. Based on this, we suggest that Chol_H is suitable for our MLE with MProp and MLE with CG-APG, and $\mathcal{A}[\cdot]_1$ for LRE, and follow these in subsequent experiments.

C. Performance comparison of various QST algorithms on 10-qubit states

Then, we employ quantum fidelity, convergence time, and iteration step of the QST algorithms, as figure of merits, to evaluate the tomography performance of MLE, LRE, and their variants on 10-qubit states. For the commonly-used MLE, our MLE with UGD (using Chol_H), MLE with CG-APG (using Chol_H), and iMLE are considered. Furthermore, in addition to the standard LRE with $\mathcal{F}[\cdot]$, we also compare the LRE based on the mapping method $\mathcal{A}[\cdot]_1$.

These QST methods are tested via the task of reconstructing the randomly generated 10-qubit Werner states, subjected to the sample noise. As illustrated in Fig. 5(a), our MLE with UGD admits a higher fidelity than MLE with CG-APG and LRE, except for iMLE which does not achieve fidelity of 0.99 within 1000 iterations under noiseless. The unified strategy $\mathcal{A}[\cdot]_1$ similarly improves the fidelity of LRE as before, but still below other MLE algorithms. And the increase in the number of samples naturally improves the tomography of the QST algorithms. Furthermore, it is shown in Fig. 5(b) that our MLE with UGD needs less iterations than iMLE and consumes an order of magnitude less time than MLE with CG-APG. It is noted that iMLE is fast to accomplish the tomography task, however, it does not achieve the fidelity of 0.99 within 1000 iterations, as evidenced in Sec. IV D. The LRE has no need for iterations and is particularly fast, at the cost of achieving relatively lower fidelity. Thus, there exist some tradeoff between time, iteration, and fidelity for these QST methods, which deserves further exploration in the future work.

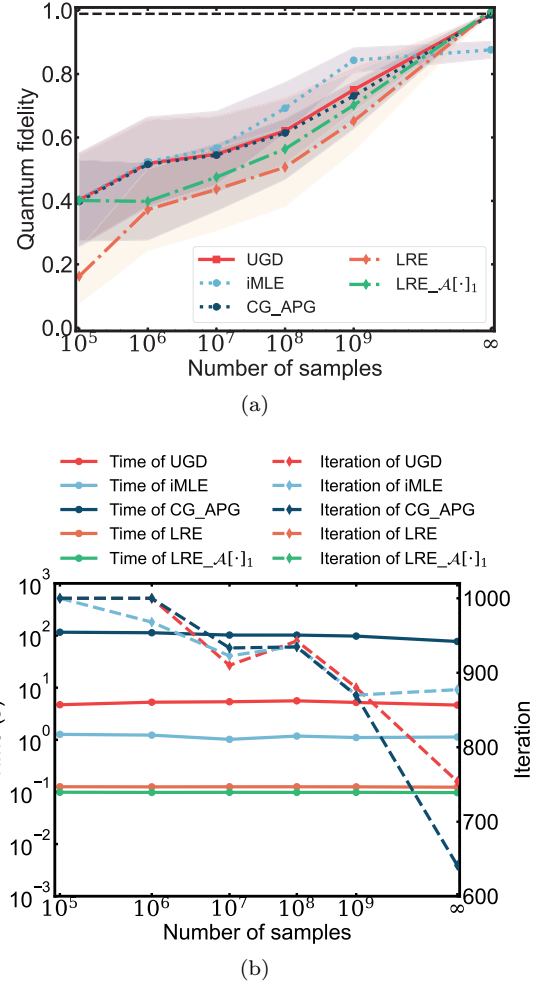


FIG. 5. The tomography performance of MLE with UGD, iMLE, MLE with CG-APG, and two LREs: the tomography fidelity (a) and the convergence time and iteration (b). Given the fixed sample size, each experiment is performed to tomography 30 random 10-qubit Werner states. Each data represents the mean fidelity and the shaded area is the half standard deviation around the mean.

D. Tomography speed of QST algorithms on numbers of qubits

We further use the convergence time and iteration to quantify the tomography speed of the QST methods. Specifically, the maximal number of iteration is set to 10^4 and there is no sample noise.

It follows from Fig. 6 that, MLE with UGD is able to tomography multi-qubit states of up to 11 within one minute, implying the scalability of our algorithm. It outperforms MLE with CG-APG and iMLE that it takes one or two orders of magnitude less time than MLE with CG-APG for 9- and 10-qubit states and iMLE for the state with larger than 6 qubits. Our UGD with MProp algorithm shows excellent scalability on a large number of qubits (> 8), with better number of iterations and

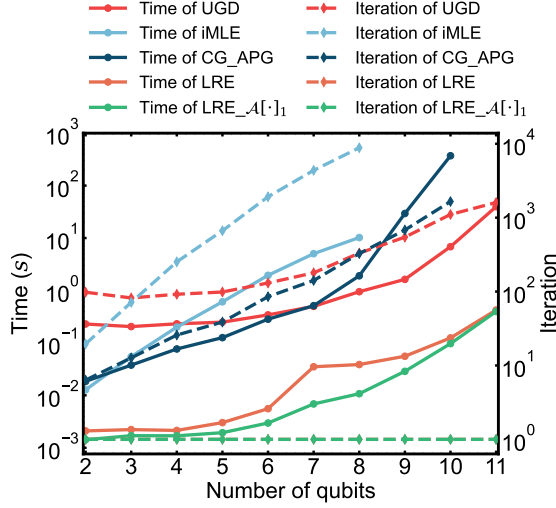


FIG. 6. The tomography speed of our MLE with UGD and other QST algorithms with the varying number of qubits. Numerical experiments are implemented to reconstruct Werner states with uniformly distributed p on average. A data point is obtained by averaging either the time or number of iteration over 30 randomly generated states. The iMLE is up to 9-qubit states as it cannot achieve the desired fidelity of 0.99 within 10^4 iterations, while the MLE with $\mathcal{A}[\cdot]_3$ needs an amount of time to reach convergence.

time than CG-APG algorithm, iMLE is eliminated due to super slow convergence. Finally, it is worth noting that although LRE is faster than our MLE with UGD, it gives rise to the reconstructed state with a relatively lower fidelity, which has been detailed in above Sec. IV C.

E. Robustness of QST algorithms towards depolarizing noise

Finally, we investigate the robustness of various QST algorithms against depolarizing noise. Indeed, this noise may change any target state into the maximally mixed state with a certain probability, which can be model as per Eq. (18) with strength λ . And the measurement statistics are obtained by measuring the pure state going through depolarizing channel with 10^6 and 10^7 times.

As shown in Fig. 7, it is evident that the presence of depolarizing noise linearly reduces the tomography fidelity of all QST. Moreover, under the same experiment setting, these algorithms, except for LRE, can reconstruct the target state with ideal fidelity $1 - (1 - 1/2^{10})\lambda$ for all noise strength λ under 10^7 samples, and the increase in samples naturally improves the noise robustness. It is also found that the unified mapping technique $\mathcal{A}[\cdot]_1$ leads to a worse performance for LRE.

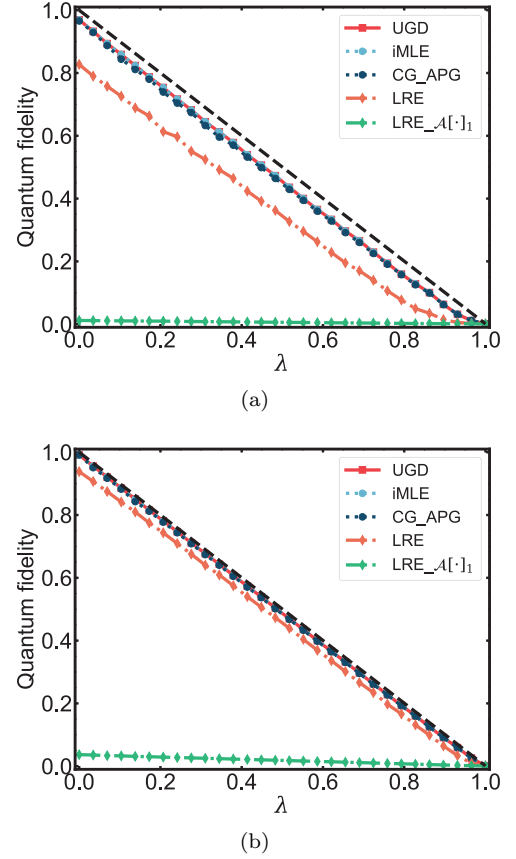


FIG. 7. The depolarizing noise robustness of our MLE with UGD and other QST algorithms. Numerical experiments are implemented to tomography 10-qubit Werner states with uniformly distributed p , and there are total 30 randomly generated states subjected to depolarizing noise (18) and the sample size of 10^6 (a) and 10^7 (b) for each algorithm. The black dotted line describes the ideal fidelity $1 - (1 - 1/2^{10})\lambda$, when the QST algorithm perfectly reconstructs the mixed state going through depolarizing noise.

V. CONCLUSION AND OUTLOOK

We have presented the MLE with the unified factored and projected gradient algorithm, which employs a unified state-mapping technique (14) and a momentum-accelerated Rprop gradient algorithm to achieve fast and robust estimation of multi-qubit mixed states. In terms of state-mapping strategies and other QST methods, numerous numerical results show that our scheme effectively combats the rank-deficient issue and thus achieves strong robustness to the state purity and noise, and more precise tomography in less time and iteration. It is demonstrated that we can perform the tomography task of 11-qubit mixed states in less than one minute. Furthermore, it is found that with respect to the MLE with UGD, the depolarizing noise linearly reduces its tomography fidelity. Importantly, our unified state-mapping strategy play a performance improvement on other QST algorithms as well.

There are many interesting questions left for the future work. For instance, we find that suitable constructions of the matrices of factored method effectively attenuate the rank-deficient issue, and find that constructions other than Hermitian form facilitate the understanding of new unified mapping strategies. Second, the validation of this paper is based on numerical experiments, and it is interesting to demonstrate theoretically the convergence property of the MLE with UGD. Finally, it is amusing to test the convergence and robustness of our algorithm on real experimental setups.

ACKNOWLEDGMENTS

We thank Dr. Changkang Hu for useful discussions. This research is supported by the National Natu-

ral Science Foundation of China (12205219, 61903027, 72171172, 62088101); the National Key R&D Program of China (2018YFE0105000, 2018YFB1305304); the Shanghai Municipal Science and Technology Major Project (2021SHZDZX0100); the Shanghai Municipal Commission of Science and Technology (1951113210, 19511132101); the Shanghai Research Institute of China Engineering Science and Technology Development Strategy, Strategic Research and Consulting Project (2022-DFZD-33-02); the Shanghai Municipal Science and Technology Fundamental Project (21JC1405400); and the Chinese Academy of Engineering, Strategic Research and Consulting Program (2022-XY-100).

-
- [1] H. Barnum and A. Wilce, Local tomography and the jordan structure of quantum theory, *Found. Phys.* **44**, 192 (2014).
 - [2] M. Baur, A. Fedorov, L. Steffen, S. Filipp, M. P. da Silva, and A. Wallraff, Benchmarking a quantum teleportation protocol in superconducting circuits using tomography and an entanglement witness, *Phys. Rev. Lett.* **108**, 040502 (2012).
 - [3] D. Cruz, R. Fournier, F. Gremion, A. Jeannerot, K. Komagata, T. Tosić, J. Thiesbrummel, C. L. Chan, N. Macris, M.-A. Dupertuis, *et al.*, Efficient quantum algorithms for ghz and w states, and implementation on the ibm quantum computer, *Adv. Quantum Technol.* **2**, 1900015 (2019).
 - [4] H.-Y. Huang, R. Kueng, and J. Preskill, Predicting many properties of a quantum system from very few measurements, *Nat. Phys.* **16**, 1050 (2020).
 - [5] Z. Hradil, Quantum-state estimation, *Phys. Rev. A* **55**, R1561 (1997).
 - [6] K. Banaszek, G. M. D'Ariano, M. G. A. Paris, and M. F. Sacchi, Maximum-likelihood estimation of the density matrix, *Phys. Rev. A* **61**, 010304 (1999).
 - [7] Y.-L. Seah, J. Shang, H. K. Ng, D. J. Nott, and B.-G. Englert, Monte carlo sampling from the quantum state space. ii, *New J. Phys.* **17**, 043018 (2015).
 - [8] G. B. Silva, S. Glancy, and H. M. Vasconcelos, Investigating bias in maximum-likelihood quantum-state tomography, *Phys. Rev. A* **95**, 022107 (2017).
 - [9] C. A. Riofrio, D. Gross, S. T. Flammia, T. Monz, D. Nigg, R. Blatt, and J. Eisert, Experimental quantum compressed sensing for a seven-qubit system, *Nat. Commun.* **8**, 15305 (2017).
 - [10] A. Kyriallidis, A. Kalev, D. Park, S. Bhojanapalli, C. Caramanis, and S. Sanghavi, Provable compressed sensing quantum state tomography via non-convex methods, *npj Quantum Inform.* **4**, 36 (2018).
 - [11] S. Ahmed, C. Sánchez Muñoz, F. Nori, and A. F. Kockum, Quantum state tomography with conditional generative adversarial networks, *Phys. Rev. Lett.* **127**, 140502 (2021).
 - [12] H. Ma, D. Dong, I. R. Petersen, C.-J. Huang, and G.-Y. Xiang, A comparative study on how neural networks enhance quantum state tomography 10.48550/arXiv.2111.09504 (2021), arXiv:2111.09504.
 - [13] D. Koutný, L. Motka, Z. c. v. Hradil, J. Řeháček, and L. L. Sánchez-Soto, Neural-network quantum state tomography, *Phys. Rev. A* **106**, 012409 (2022).
 - [14] J. A. Smolin, J. M. Gambetta, and G. Smith, Efficient method for computing the maximum-likelihood quantum state from measurements with additive gaussian noise, *Phys. Rev. Lett.* **108**, 070502 (2012).
 - [15] B. Qi, Z. Hou, L. Li, D. Dong, G. Xiang, and G. Guo, Quantum state tomography via linear regression estimation, *Sci Rep* **3**, 3496 (2013).
 - [16] B. Qi, Z. Hou, Y. Wang, D. Dong, H.-S. Zhong, L. Li, G.-Y. Xiang, H. M. Wiseman, C.-F. Li, and G.-C. Guo, Adaptive quantum state tomography via linear regression estimation: Theory and two-qubit experiment, *npj Quantum Inform.* **3**, 19 (2017).
 - [17] E. Bolduc, G. C. Knee, E. M. Gauger, and J. Leach, Projected gradient descent algorithms for quantum state tomography, *npj Quantum Inform.* **3**, 44 (2017).
 - [18] V. Siddhu, Maximum a posteriori probability estimates for quantum tomography, *Phys. Rev. A* **99**, 012342 (2019).
 - [19] J. M. Lukens, K. J. Law, A. Jasra, and P. Lougovski, A practical and efficient approach for bayesian quantum state estimation, *New J. Phys.* **22**, 063038 (2020).
 - [20] R. Blume-Kohout, Hedged maximum likelihood quantum state estimation, *Phys. Rev. Lett.* **105**, 200504 (2010).
 - [21] R. Blume-Kohout, Optimal, reliable estimation of quantum states, *New J. Phys.* **12**, 043034 (2010).
 - [22] T. Baumgratz, A. Nüßeler, M. Cramer, and M. B. Plenio, A scalable maximum likelihood method for quantum state tomography, *New J. Phys.* **15**, 125004 (2013).
 - [23] Z. Hou, H.-S. Zhong, Y. Tian, D. Dong, B. Qi, L. Li, Y. Wang, F. Nori, G.-Y. Xiang, C.-F. Li, *et al.*, Full reconstruction of a 14-qubit state within four hours, *New J. Phys.* **18**, 083036 (2016).
 - [24] D. Gross, Y.-K. Liu, S. T. Flammia, S. Becker, and J. Eisert, Quantum state tomography via compressed sensing, *Phys. Rev. Lett.* **105**, 150401 (2010).

- [25] G. Tóth, W. Wiczeorek, D. Gross, R. Krischek, C. Schwemmer, and H. Weinfurter, Permutationally invariant quantum tomography, *Phys. Rev. Lett.* **105**, 250403 (2010).
- [26] M. Christandl and R. Renner, Reliable quantum state tomography, *Phys. Rev. Lett.* **109**, 120403 (2012).
- [27] M. Cramer, M. B. Plenio, S. T. Flammia, R. Somma, D. Gross, S. D. Bartlett, O. Landon-Cardinal, D. Poulin, and Y.-K. Liu, Efficient quantum state tomography, *Nat. Commun.* **1**, 149 (2010).
- [28] T. Baumgratz, D. Gross, M. Cramer, and M. B. Plenio, Scalable reconstruction of density matrices, *Phys. Rev. Lett.* **111**, 020401 (2013).
- [29] B. Lanyon, C. Maier, M. Holzäpfel, T. Baumgratz, C. Hempel, P. Jurcevic, I. Dhand, A. Buyskikh, A. Daley, M. Cramer, *et al.*, Efficient tomography of a quantum many-body system, *Nat. Phys.* **13**, 1158 (2017).
- [30] G. Torlai, G. Mazzola, J. Carrasquilla, M. Troyer, R. Melko, and G. Carleo, Neural-network quantum state tomography, *Nat. Phys.* **14**, 447 (2018).
- [31] A. Rocchetto, E. Grant, S. Strelchuk, G. Carleo, and S. Severini, Learning hard quantum distributions with variational autoencoders, *npj Quantum Inform.* **4**, 28 (2018).
- [32] P. Cha, P. Ginsparg, F. Wu, J. Carrasquilla, P. L. McMahon, and E.-A. Kim, Attention-based quantum tomography, *Mach Learn: Sci. Technol.* **3**, 01LT01 (2021).
- [33] J. Řeháček, Z. c. v. Hradil, E. Knill, and A. I. Lvovsky, Diluted maximum-likelihood algorithm for quantum tomography, *Phys. Rev. A* **75**, 042108 (2007).
- [34] J. Shang, Z. Zhang, and H. K. Ng, Superfast maximum-likelihood reconstruction for quantum tomography, *Phys. Rev. A* **95**, 062336 (2017).
- [35] J. L. Kim, G. Kollias, A. Kalev, K. X. Wei, and A. Kyrillidis, Fast quantum state reconstruction via accelerated non-convex programming, *Photonics* **10**, 116 (2023).
- [36] C.-E. Tsai, H.-C. Cheng, and Y.-H. Li, Faster Stochastic First-Order Method for Maximum-Likelihood Quantum State Tomography 10.48550/arXiv.2211.12880 (2022), arXiv:2211.12880.
- [37] M.-C. Hsu, E.-J. Kuo, W.-H. Yu, J.-F. Cai, and M.-H. Hsieh, Quantum state tomography via non-convex Riemannian gradient descent 10.48550/arXiv.2210.04717 (2022), arXiv:2210.04717.
- [38] A. I. Lvovsky, Iterative maximum-likelihood reconstruction in quantum homodyne tomography, *J. Opt. B-Quantum Semicl. Opt.* **6**, S556 (2004).
- [39] D. S. Gonçalves, M. A. Gomes-Ruggiero, and C. Lavor, Global convergence of diluted iterations in maximum-likelihood quantum tomography, *Quantum Info. Comput.* **14**, 966–980 (2014).
- [40] A. Farooq, U. Khalid, J. ur Rehman, and H. Shin, Robust quantum state tomography method for quantum sensing, *Sensors* **22**, 2669 (2022).
- [41] A. Keselman, Y. Glickman, N. Akerman, S. Kotler, and R. Ozeri, High-fidelity state detection and tomography of a single-ion zeeman qubit, *New J. Phys.* **13**, 073027 (2011).
- [42] K. J. Resch, P. Walther, and A. Zeilinger, Full characterization of a three-photon greenberger-horne-zeilinger state using quantum state tomography, *Phys. Rev. Lett.* **94**, 070402 (2005).
- [43] R. Jozsa, Fidelity for mixed quantum states, *J. Mod. Opt.* **41**, 2315 (1994).
- [44] C. Igel and M. Hüsken, Empirical evaluation of the improved rprop learning algorithms, *Neurocomputing* **50**, 105 (2003).
- [45] Y. Wang, Qst-ugd—open source github repository (2023), accessed 20 June 2023. <https://github.com/foxwy/QST-UGD>.
- [46] J. Řeháček, Z. c. v. Hradil, E. Knill, and A. I. Lvovsky, Diluted maximum-likelihood algorithm for quantum tomography, *Phys. Rev. A* **75**, 042108 (2007).